Observation of high-contrast coherence fringes in high-order harmonic generation

S. Kazamias, D. Douillet, C. Valentin, F. Weihe, F. Augé, Th. Lefrou, G. Grillon, S. Sebban, and Ph. Balcou
Laboratoire d'Optique Appliquée, ENSTA-Ecole Polytechnique, Centre National de la Recherche Scientifique, UMR 7639, F-91761 Palaiseau cedex, France

(Received 28 May 2003; published 29 September 2003)

We present a direct measurement of the coherence length in the high-order-harmonic generation process up to orders as high as 25. The harmonic signal generated in an argon gas cell by a 805-nm, 6-mJ, 30-fs laser is studied as a function of medium length and shows very high-contrast coherence fringes. From a one-dimensional time-dependent model, we unravel the conditions for which such Maker fringes can appear in high-order harmonic generation.

DOI: 10.1103/PhysRevA.68.033819 PACS number(s): 42.65.Ky, 32.80.Rm, 42.65.Re

I. INTRODUCTION

High-order harmonic generation (HHG) is now an efficient way to generate coherent radiation in the extreme ultraviolet (euv) spectral range from 10 to 40 nm [1]. High conversion efficiencies are obtained by focusing an ultrashort and intense infrared laser beam on a rare-gas target, typically a gas cell [2] or a gas-filled capillary waveguide [3]. High-order-harmonic generation is then the result of the highly nonlinear interaction between the short-pulse-high-intensity-laser and the gas medium.

The efficiency of the process is the result of both microscopic and macroscopic considerations. The microscopic polarization comes from the quantum interaction between a single atom and the high electric field of the laser [4]. As was stressed since the earlier time of nonlinear optics [5], the macroscopic response of a nonlinear medium results from the phase matching inside it: the signal is optimized when the wave-vector mismatch is equal to zero. The latter is defined as $\delta k = k_q - q k_1$, where q is the harmonic order and k_1 and k_q are the wave vectors for the fundamental and harmonic radiation, respectively. In the case of a non-phase-matched, nonabsorbing medium of length L, the signal at the exit is proportional to $L^2([\sin(\delta kL/2)]/\delta kL/2)^2$ [6]. The signal variation as a function of medium length presents some oscillations characterized by the so-called coherence length (l_{coh} in the following) which is the length over which the harmonic signal can build up constructively. If the medium length becomes higher than the coherence length, destructive interferences occur and lead to coherence fringes, also called Maker fringes [5]. This coherence criterion was first observed experimentally for a low harmonic order (H3) generated in gases by Puell *et al.* [6].

This Maker fringe behavior is simple to observe in the low intensity regime of nonlinear optics. In the strong-field regime reached nowadays and leading to the phenomena of HHG, it is far more difficult to observe experimentally for many reasons, among which the rather complicated dependence of phase matching on time and space. Moreover, one of the best candidates for homogeneous phase matching is the use of capillary waveguides whose length is impossible to change easily to see coherence fringes. To our knowledge, direct and precise characterization of coherence fringes by detecting a spatial periodicity of harmonic signal was made only once by L'Huillier *et al.* [7]. The harmonic orders considered and the pump-laser characteristics were nevertheless quite far from those commonly studied now, as those authors were studying harmonics $H9$ to $H13$ of a 1064-nm, 40-ps pulse duration laser. In recent experiments in which efficient harmonic generation was obtained up to very high orders, such as reported in Ref. [8], a rough estimate of a minimum value for the coherence length is usually given by the medium length for which a saturation of the harmonic photon flux is observed. Strikingly, no other report of coherence oscillations in HHG were reported in the last ten years.

In a recent paper [2], we presented a study on global optimization of high harmonic generation based on the observation of Maker fringes, which allowed us to find the best conditions for phase matching. The present article consists of a more complete study of the coherence fringes phenomena in itself. We show fringes from high harmonic orders ($H17$ to $H27$) obtained in argon with a 805-nm, 30-fs pulse duration laser in experimental conditions close to optimization. We then concentrate on the experimental determination of the coherence length and explain the influence of important parameters by presenting a set of experimental Maker fringes in different generation conditions.

The paper is presented as follows. In Sec. II, we show the experimental results and outline the conditions in which they were obtained. After recalling in Sec. III the basic equations describing phase matching in a one-dimensional (1D) model of high harmonic generation, we describe in Sec. IV the conditions required for observing high-contrast coherence fringes. In Sec. V, we show that the observation of Maker fringes allows us to better understand the role of parameters such as the quantum path on the phase matching of high-order harmonics.

II. EXPERIMENTAL EVIDENCE OF HIGH-CONTRAST MAKER FRINGES

A. Experimental setup

We have performed the study of coherence effects on the high harmonic orders generated by a Ti:sapphire laser system delivering a train of 6-mJ, 30-fs pulses with a center wavelength of 805 nm at a repetition rate of 1 kHz. The important elements of the generation setup are presented in Fig. 1: the infrared beam is first apertured to half of its waist (11 mm

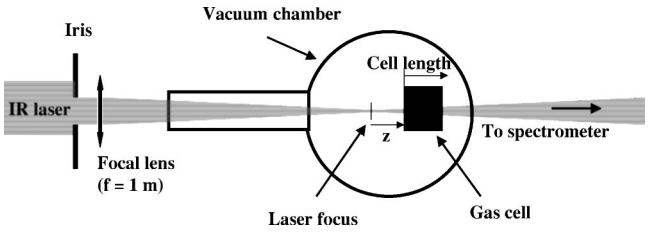

FIG. 1. Experimental high harmonic generation setup.

diameter) before being focused by a 1 m focal length M_gF_2 lens [9] to avoid any nonlinear effect within the optical component. The resulting Rayleigh range (z_0) is 17 mm and guarantees a loose focusing geometry within the generating medium.

The gas medium is composed by a varying length gas cell that plays a central role for the phase-matching study: whereas the entrance of the cell is fixed, the exit is motorized so that the cell length can vary from 0 to 7 mm with an absolute accuracy better than 0.2 mm. The gas pressure is an adjustable parameter between 0 and 50 torr and is calibrated in absolute value by a piezoelectric pressure transducer. The lens is also motorized so that the cell entrance position relative to the laser focus can be simply modified. In the following, we will call z the distance between laser focus and cell entrance with the convention that $z>0$ means the cell is placed after the focus (see Fig. 1). The harmonic generation setup is placed in a vacuum chamber ($P<10^{-3}$ mbar) to avoid any absorption of the euv radiation.

The harmonics are emitted collinearly with the infrared laser and the latter has to be eliminated before the harmonics are sent into the spectrometer. This is technically done by the use of two 125-nm thick aluminum filters whose transmission is 20% in the 30 nm wavelength range and 0 for the infrared beam. The spectrometer is composed of a spherical gold mirror and a transmission grating (2000 grooves per mm) that separates all harmonic orders with the same spectral efficiency (3% for the first diffraction order). The harmonic spectra are recorded with an extreme ultraviolet–charge-coupled device (XUV-CCD) camera and the acquisition times depend on the harmonic flux. The typical values are from 0.1 to 1 s and represent 100 to 1000 laser shots, leading to reduced statistical uncertainties.

B. Experimental results

Figures 2 and 3 show the harmonic signal obtained in 15 torr of argon by varying the medium length from 0 to 7 mm by 0.5 mm steps. In Fig. 2, the cell entrance is either placed 2 mm before or after the laser focus, corresponding to full circles and triangles, respectively, and the laser intensity is 3×10^{14} W/cm^2. The behavior of the fringe contrast is radically different between the two cases. Whereas the case $z=+2$ mm shows a quasiregular growth of the harmonic signal with the cell length followed by a saturation, the case $z=-2$ mm shows a periodic variation with highly contrasted fringes. The ratio between the maximum and the minimum of the curve is indeed up to a factor of 100 for harmonic 25. The experimental instability of the harmonic flux is evaluated to 30% and cannot be the explanation for such high-contrast periodic fringes. We can conclude that the observed period of the phenomena is 1.5 mm, which corresponds to twice the effective coherence length ($l_{coh}=0.75$ mm). The number of emitted photons is also completely different: it is 2 to 100 times higher when the cell is placed after the focus, where no fringes appear.

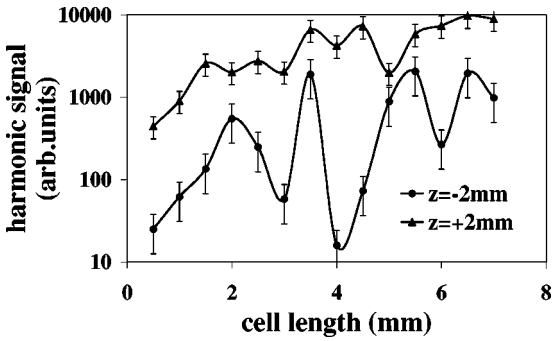

FIG. 2. Harmonic signal as a function of the medium length obtained for the 25th order generated in 15 torr of argon. The full circles represent the experimental points for a cell entrance placed 2 mm before the focus ($z=-2$ mm), whereas the triangles represent a cell entrance placed after the focus ($z=+2$ mm).

The fringe behavior for different harmonic orders is presented in Fig. 3. Within the step resolution for the medium length (0.5 mm), the coherence length itself seems unchanged, whereas the influence of harmonic order is clearly visible in the contrast ratio: the contrast is only 10 for $H17$ generated in argon and it grows to 100 for $H25$. This behavior is close to the theoretical prediction for the contrast of harmonic 3 presented in Ref. [10]. From that study, the absorption length of the atomic medium can be expected to play a role that will be discussed in Sec. IV.

This unexpected high-contrast level for coherence fringes will be studied in the following sections. We will first develop a one-dimensional time-dependent harmonic generation model based on phase-matching considerations, which allows one to understand the origin of Maker fringes. From the dependence of some relevant parameters on time and space, we will then exhibit possible sources of a reduced contrast. This will explain why our experimental conditions are particularly adapted for this observation.

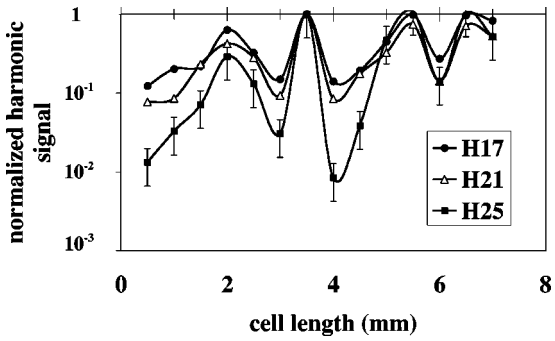

FIG. 3. Harmonic signal as a function of the medium length for different harmonic orders generated in argon from 17th (circles), to 21st (triangles) and 25th (squares). The gas pressure is 10 torr and the cell entrance is placed 2 mm before the laser focus.

III. COHERENCE FRINGES IN A TIME-INDEPENDENT MODEL

For the sake of completeness, we first recall the basics of phase matching in a one-dimensional time-independent model in the spirit of Refs. [11,12]. The role of the coherence length will then be underlined.

The harmonic emission is the result of the laser-induced nonlinear polarization up to high orders. Each gas atom behaves as a small dipole [4] so that the qth harmonic field at the exit of the medium is the integral of all of these atomic dipoles along the medium. In the case of an absorbing medium, the resolution of the paraxial Maxwell equations with a high-harmonic polarization term leads to the following expression for the instantaneous harmonic field [2]:

$$E_q(l_{med}) = \frac{iq\omega}{\epsilon_0 c}\int_0^{l_{med}} d_q(z)\exp\left(\frac{z-l_{med}}{2l_{abs}}\right)\exp[i\phi_q(z)]dz, \tag{1}$$

where l_{med} is the medium length, l_{abs} is the absorption length and characterizes the distance over which a harmonic radiation is reduced by a factor of $1/e$, $d_q(z)$ is the amplitude of the high harmonic dipole, $\phi_q(z)$ is the total propagation dephasing between the harmonic radiation and the laser induced polarization at the exit of the medium, c and ϵ_0 are, respectively, the speed of light and vacuum permittivity, and ω is the infrared angular frequency.

The dipole amplitude can be calculated in the full quantum theory of Lewenstein [4,13]. The dependence on laser intensity can be properly fitted by a fifth-order power law, which we consider in the following. The most important feature of Refs. [4,13] is the existence of two different quantum paths that contribute to a given harmonic order, each with its own intensity-dependent quantum phase. Based on the saddle-point approximation, Lewenstein *et al.* demonstrated that the quantum phases depend linearly on the laser intensity I: the first one with a small coefficient ($\phi_{at_1} \approx -10^{-14} I(\mathrm{cm}^2/\mathrm{W})$) and the second one with a more important one [$\phi_{at_2} \approx -25\times 10^{-14} I(\mathrm{cm}^2/\mathrm{W})$]. This phase effect has an influence on phase matching as was shown in Refs. [14,15]. The phase matching is indeed characterized by the phase term $\phi_q(z)$ which depends on quantum path.

If the generating conditions can be considered homogeneous all over the medium, the phase term reads as

$$\phi_q(z) = k_q\cdot z - qk_1\cdot z + \phi_{at} = \delta k\cdot z = \frac{\pi z}{l_{coh}}, \tag{2}$$

where k_q and k_1 are the wave vectors for the harmonic radiation and the infrared laser, respectively; ϕ_{at} is the atomic phase for either the first or the second quantum path. In the case where l_{coh} is constant, Eq. (1) can be integrated analytically, so that the number of photons emitted on axis per unit time and area is proportional to [12]

$$N_{out}(l_{med}) \propto d_q^2 \frac{4l_{abs}^2}{1+4\pi^2\dfrac{l_{abs}^2}{l_{coh}^2}}\left[1+\exp\left(-\frac{l_{med}}{l_{abs}}\right) - 2\cos\left(\frac{\pi l_{med}}{l_{coh}}\right)\exp\left(\frac{-l_{med}}{2l_{abs}}\right)\right]. \tag{3}$$

The cosine term in Eq. (3) clearly induces oscillations in the signal as a function of l_{med}, known as Maker fringes. The fringe contrast ratio itself clearly depends on the absorption length through the exponential term.

IV. REQUIREMENTS FOR THE OBSERVATION OF MAKER FRINGES

The appearance of Maker fringes is commonplace in standard nonlinear optics; the puzzling point is why such fringes were so rarely detected in experiments of high harmonic generation. In the following sections we will study the variations of the coherence length both in time and space to understand the role of these variations on the fringe contrast.

A. Spatial variation of the coherence length

One fundamental condition for observing high-contrast fringes is the existence of a well defined coherence length all over the medium at a given time in the pulse. If this condition is not fulfilled the contrast will be strongly deteriorated. Equation (2) gives the relation between the dephasing gradient and the coherence length: $l_{coh} = \pi/(\partial\phi/\partial z)$. Having a constant coherence length thus means a constant phase slope.

The phase mismatch can be calculated for each point in the cell: it is given by the contribution of the electronic and atomic dispersion terms and also atomic and geometrical phase gradients [15]. Using usual notations, the phase slope reads as

$$\delta k = k_q - qk_1 + \nabla\phi_{at} = q\frac{\omega}{c}\left(\frac{n_e}{2n_c} - (n_{at}-1)\right) + q\nabla\phi_G + \nabla\phi_{at}, \tag{4}$$

where n_e is the electronic density and n_c the critical density for the plasma created by the laser, n_{at} is the index of refraction of the neutral gas, Φ_G represents the Gouy phase experienced by the pump laser as it is focused in the cell [14,16].

A homogeneous phase slope means first that the electronic density is constant over the cell, second that the Gouy phase and atomic phase gradients are constant too. The condition on electronic density is fulfilled when the laser intensity is constant over the medium so that the ionization level is spatially unchanged. At the same time, the atomic phase gradient [13] and the Gouy phase gradient are also very weak. This happens when the Rayleigh range (z_0) of the infrared laser is much longer than the medium length itself [2].

Figures 4(a) and 4(b) illustrate this by showing the dephasing calculated from the commonly used ADK (Ammosov, Delone, and Krainov) ionization rates [17] for the 27th harmonic order generated in a 5 mm long cell filled

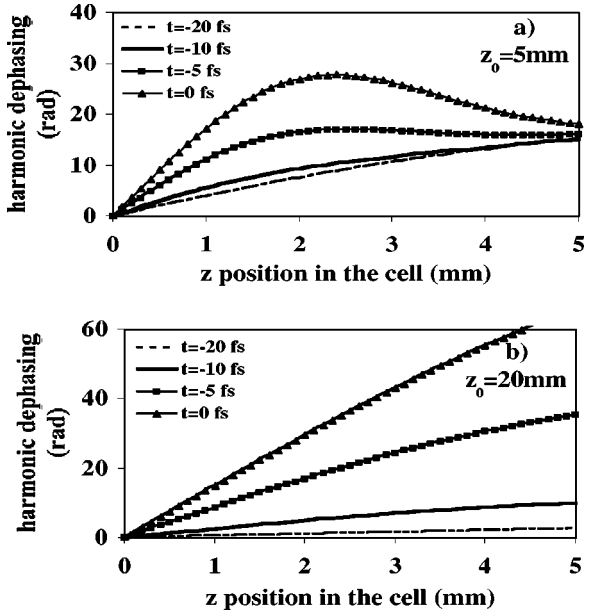

FIG. 4. Spatial variation of the dephasing experienced by $H27$ generated in 10 torr of argon, the cell is at focus so that only the first quantum path is considered. The maximum intensity is 3×10^{14} W/cm^2 (pulse duration 30 fs). Different times in the pulse are represented: 20 fs before the maximum (dotted line), 10 fs before (thick line), 5 fs (full squares), and the maximum itself (full triangles); (a) corresponds to a 5-mm Rayleigh range and (b) to a 20-mm one.

with 10 torr of argon. Each curve represents a specific time in the pulse compared to the maximum, the pulse duration being 30 fs. Figure 4(a) corresponds to a Rayleigh range equal to the cell length and shows a nonconstant phase slope, especially near the maximum of the pulse where the ionization plays an important role. On the contrary, Fig. 4(b) shows that a Rayleigh range equal to four times the cell length is appropriate for linear phase and allows one to define a clear coherence length, although it still depends on time.

Figure 5 shows the instantaneous H27 harmonic flux as a function of medium length for $t=-5$ fs, inferred from Eq. (1) and the phase variations of Figs. 4(a) and 4(b). As expected, the contrast ratio is much higher in the case of a 20-mm Rayleigh range (black line) than in the case of a

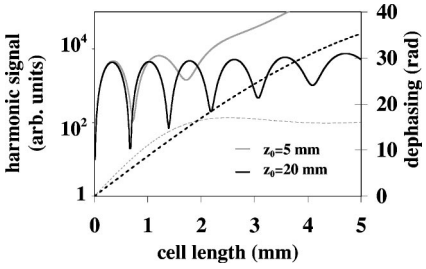

FIG. 5. Instantaneous harmonic signal for $H27$ at $t=-5$ fs vs the medium length inferred from the phase variations of Figs. 4(a) and 4(b), gray line corresponds to $z_0=5$ mm, black line to $z_0=20$ mm. The dotted lines represent the corresponding phase variations in radians (gray line: $z_0=5$ mm, black line: $z_0=20$ mm).

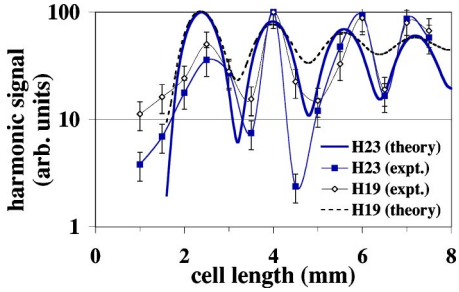

FIG. 6. Harmonic signal vs the medium length for harmonic 23rd (full squares) and 19th (full diamonds). The experimental results are compared to theoretical prediction following Eq. (3), where l_{coh} is taken equal to 0.8 mm and l_{abs} is 1.08 mm for $H19$ and 2.19 mm for $H23$. The generation conditions are the same as for Fig. 2.

reduced one (gray line for $z_0=5$ mm), for which we observe a nonlinear phase variation within the cell. As was shown in Ref. [9], the use of an iris to aperture the beam, before it is focused into the cell, can increase considerably the Rayleigh range of the infrared laser and guarantees homogeneous phase matching.

In the experimental conditions for which we observed Maker fringes, the iris aperture was 11 mm in diameter and the resulting Rayleigh range was up to 17 mm. We also checked that increasing the iris aperture makes the fringes disappear. In conclusion, a large Rayleigh range is required to observe fringes. The development in recent years of high energy (several mJ), ultrashort, high repetition rate systems favors such loose focusing geometries, using either very long focusing [18,19] and/or aperturing the beam [9].

B. Influence of the absorption length on the contrast

In recent analysis of optimized HHG, it was underlined that generation should happen in a strongly saturated regime, i.e., when the medium length is much longer than the absorption length, and the coherence length longer than the medium length [8,11,12]. In contrast, we have observed the highest contrast fringes in conditions where the coherence is smaller than the maximum medium length, thus out of the strongly saturated regime.

Figure 6 shows, for instance, the comparison between experimental signal and theoretical prediction following Eq. (3) for harmonic orders 19 and 23 generated in the conditions of Fig. 2 for which the coherence length is experimentally equal to 0.75 mm. The absorption lengths involved are 1.08 mm for $H19$ and 2.19 mm for $H23$; they were computed from Ref. [20]. As can be seen in Fig. 6, both the experimental and the theoretical fringe contrasts are strongly influenced by the harmonic order considered: the contrast increases impressively with the order.

The reason for such behavior can be understood by studying the theoretical contrast C defined as the ratio between the first maximum of the signal (corresponding to a cell length equal to l_{coh}) and the first minimum (corresponding to a cell length equal to $2l_{coh}$). C can be analytically calculated from Eq. (3):

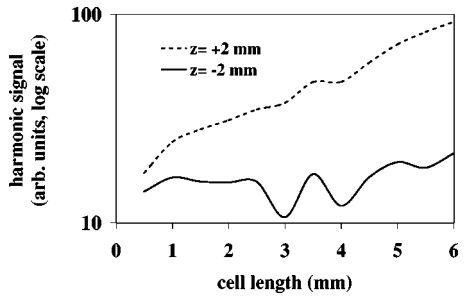

FIG. 7. Numerical simulations of the 25th harmonic signal as a function of the cell length. The conditions are the experimental conditions of Fig. 1. Dotted line represents a cell entrance placed 2 mm after the laser focus ($z=+2$ mm), the full line represents a cell entrance placed 2 mm before the focus ($z=-2$ mm).

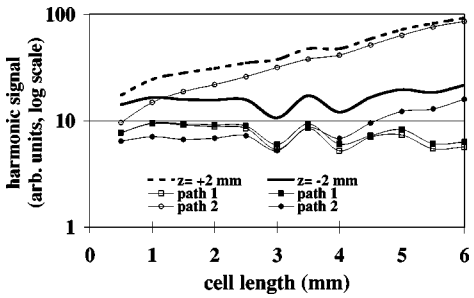

FIG. 8. Numerical simulations of the 25th harmonic signal as a function of the cell length. The conditions are the same as for Fig. 7 but the contribution of each quantum path is separately shown (dotted line, total signal for $z=+2$ mm; open squares, first quantum path; open circles, second quantum path; full line, total signal for $z=-2$ mm; full squares, first quantum path; full circles, second quantum path).

$$\mathrm{Max}(N_{out}) \propto d_q^2 \frac{4l_{abs}^2}{1+4\pi^2\frac{l_{abs}^2}{l_{coh}^2}}\left[1+\exp\left(-\frac{l_{coh}}{l_{abs}}\right)+2\exp\left(-\frac{l_{coh}}{2l_{abs}}\right)\right], \tag{5}$$

$$\mathrm{Min}(N_{out}) \propto d_q^2 \frac{4l_{abs}^2}{1+4\pi^2\frac{l_{abs}^2}{l_{coh}^2}}\left[1+\exp\left(-\frac{2l_{coh}}{l_{abs}}\right)-2\exp\left(-\frac{l_{coh}}{l_{abs}}\right)\right]. \tag{6}$$

The ratio of the two above terms can finally be expressed very simply as

$$C=\left(\frac{1+\sqrt{x}}{1-x}\right)^2, \tag{7}$$

where $x=\exp(-l_{coh}/l_{abs})$.

We conclude that high-contrast Maker fringes are only observable for harmonic orders for which the absorption length is high enough compared to the coherence length: a contrast of 10 is obtained, for example, if $l_{coh}/l_{abs}=0.8$, it would be 100 if $l_{coh}/l_{abs}=0.2$. Such values of the contrast were experimentally observed for $H25$ and $H27$ in argon for which the former condition is fulfilled.

V. ANALYSIS OF THE FRINGE BEHAVIOR REGARDING THE FOCUS POSITION

Figure 2 presents a very striking behavior of the fringes when the cell entrance position goes through the laser focus. When the cell is placed before the focus, the fringe contrast is high and the number of photons quite low. On the contrary, when the cell is placed after the focus, the number of photons increases and fringes vanish.

This result is qualitatively reproduced in Fig. 7 by a one-dimensional time-dependent phase-matching code described in Ref. [9]. The 1D approximation is appropriate for our experimental conditions for which the Rayleigh range is large compared to the cell length and the laser intensity is moderate ($I=3\times10^{14}$ W/cm^2). In those conditions, the agreement observed between experimental and theoretical predictions from the code presented in Refs. [2,9] shows that phase matching essentially occurs on axis, which is very important for the definition of a proper coherence length. The code itself is based on the time-dependent evaluation of the dephasing, following Eq. (2). The knowledge of laser intensity and ionization level is required. We therefore consider a 30-fs duration Gaussian pulse and calculate the ionization from the ADK rates [17]. The instantaneous harmonic flux is then given by Eq. (3) and the total harmonic signal S at the end of the pulse is the sum of contributions from both the first and the second quantum paths. Following Ref. [21] and in order to underline the specific influence of phase matching, we take equivalent weights for the dipole amplitude of each path, so that

$$S=\sum_{path1,2}\int_0^{t_{pulse}} N_{out_{1,2}}(t)dt. \tag{8}$$

Although the calculated fringe contrast presented in Fig. 6 for the case $z=+2$ mm (dotted line) and $z=-2$ mm (full line) is much smaller than in Fig. 5, these calculations enable one to understand the difference between the two focus positions $z=-2$ mm and $z=+2$ mm. These two points are symmetrical from the focus and all parameters are identical except the atomic phase gradient, whose sign is opposite. The difference comes therefore from the influence of the second quantum path on phase matching. When the cell is placed before the focus, the atomic phase gradient induces a dispersion term that deteriorates phase matching, whereas it enhances phase matching when the cell is placed after the focus [2]. This leads to the fact that the first quantum path dominates when the cell is placed before the focus ($z=-2$ mm) and the second one when the cell is after the focus, the total harmonic signal being the sum of the two quantum path contributions. This result is clearly visible in Fig. 8 that represents the separate contribution of each quantum path in each focusing case. The fringes vanish for $z=$

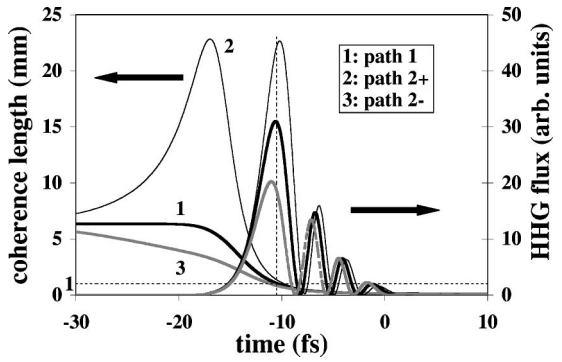

FIG. 9. Computed time dependence of the coherence length for $H25$ generated in 15 torr of argon, the laser characteristics are an intensity of 3×10^{14} W/cm^2 and a Rayleigh range of 17 mm. The thick black line represents the contribution from the first quantum path, the thin black and thick gray lines represent the second quantum path for $z=+2$ mm and $z=-2$ mm, respectively. The corresponding harmonic flux are represented with the same color code.

$+2$ mm because the second quantum path dominates and allows the effective coherence length to be higher than the medium length.

The reduced contrast for the simulated fringes arises from the time dependence of the coherence length within the pulse. It is represented in Fig. 9 for quantum paths 1 and 2 and for the two focus positions $z=+2$ and -2 mm (thin black line and thick gray line, respectively, for quantum path 2 and thick black line for quantum path 1 in both cases). For comparison, we represent the resulting instantaneous harmonic flux for $H25$ in each case. We first note that the coherence length value at the time of the maximum flux for the first quantum path contribution approximately corresponds to what was observed experimentally [$l_{coh}(t_{max})\approx1$ mm as can be seen from the dotted lines intersection]. Surprisingly, the experiment shows higher contrast level than theory: this indicates that the harmonic flux is more concentrated in time than expected from the code. The latter predicts indeed a significant variation of the coherence length at times when the harmonic flux is important, which is not consistent with the data. Moreover, the code predicts the presence of small ripples in the harmonic flux profile, equivalent to ''temporal Maker fringes'': the harmonic emission is equal to zero exactly at those times in the pulse when the medium length is a pair multiple of the coherence length [see Eq. (3)]. The fringe contrast is thus reduced by the existence of a set of coherence lengths that give rise to local maxima of the harmonic flux in the time domain. The very high contrast observed experimentally could be due to a more complex behavior of the atomic response as compared to the strong-field approximation (SFA) [4]. Recent time-dependent Schrodinger equation calculations [22] showed, for example, some discrepancies with the SFA model. From our data, we expect that refined work on HHG dipoles may predict shorter bursts of XUV polarization than currenly considered in SFA models.

VI. CONCLUSION

The detection of coherence fringes is thus an interesting way to study phase matching and in particular the specific contribution of each quantum path. We showed the importance of relevant parameters such as coherence and absorption lengths on the fringe contrast. We demonstrated how our loose focusing conditions were appropriate for the observation of coherence fringes. In order to explain the contrast observed experimentally, as compared to theoretical predictions, we suggest that the harmonic emission may be shorter in time than expected from usual pulse envelope approximation and SFA model.

Finally, we can emphasize the parallel between the conditions unraveled to observe highly contrasted Maker fringes and the conditions to obtain good phase locking of high harmonics leading to attosecond pulse trains. As was shown by Gaarde and Schafer in Ref. [23], the smoother phase behavior of the first quantum path, both in time and space, is instrumental in reaching good phase locking. We obtain similar conditions to observe contrasted fringes. We can therefore conjecture that the existence of well contrasted fringes is a sign of proper phase locking. The present study may offer an easier control than direct harmonic phase measurements for the optimized generation of attosecond pulse trains in the XUV domain.

ACKNOWLEDGMENT

We want to thank Ph. Zeitoun for the loan of the XUV-CCD camera.

[1] T. Brabec and F. Krausz, Rev. Mod. Phys. **72**, 545 (2000).
[2] S. Kazamias, D. Douillet, F. Weihe, C. Valentin, A. Rousse, S. Sebban, G. Grillon, F. Augé, D. Hulin, and Ph. Balcou, Phys. Rev. Lett. **90**, 193901 (2003).
[3] A. Rundquist, C.G. Durfee, Z. Chang, C. Herne, S. Backus, M.M. Murnane, and H.C. Kapteyn, Science **280**, 1412 (1998).
[4] M. Lewenstein, Ph. Balcou, M.Y. Ivanov, A. L'Huillier, and P.B. Corkum, Phys. Rev. A **49**, 2117 (1994).
[5] P.D. Maker, R.W. Terhune, M. Nisehoff, and C.M. Savage, Phys. Rev. Lett. **8**, 61 (1962).
[6] H. Puell, K. Spanner, W. Falkenstein, W. Kaiser, and C.R. Vidal, Phys. Rev. A **14**, 2240 (1976).
[7] A. L'Huillier, Ph. Balcou, and L. Lompré, Phys. Rev. Lett. **68**, 166 (1992).
[8] M. Schnuerer, Z. Cheng, M. Hentschel, G. Tempea, P. Kálmán, T. Brabec, and F. Krausz, Phys. Rev. Lett. **83**, 722 (1999).
[9] S. Kazamias, F. Weihe, D. Douillet, C. Valentin, T. Planchon, S. Sebban, G. Grillon, F. Augé, D. Hulin, and Ph. Balcou, Eur. Phys. J. D **21**, 353 (2002).
[10] H. Scheingraber, H. Puell, and C.R. Vidal, Phys. Rev. A **18**, 2585 (1978).
[11] C.G. Durfee, A.R. Rundquist, S. Backus, C. Herne, M.M. Murnane, and H.C. Kapteyn, Phys. Rev. Lett. **83**, 2187 (1999).
[12] E. Constant, D. Garzella, P. Breger, E. Mével, Ch. Dorrer, C.

Le Blanc, F. Salin, and P. Agostini, Phys. Rev. Lett. **82**, 1668 (1999).
[13] M. Lewenstein, P. Salières, and A. L'Huillier, Phys. Rev. A **52**, 4747 (1995).
[14] P. Salières, A. L'Huillier, and M. Lewenstein, Phys. Rev. Lett. **74**, 3776 (1995).
[15] Ph. Balcou, P. Salières, A. L'Huillier, and M. Lewenstein, Phys. Rev. A **55**, 3204 (1997).
[16] A.E. Siegman, *Lasers* (University of California, Berkeley, 1986), p. 682.
[17] N.B. Delone and V.P. Krainov, Phys. Usp. **41**, 469 (1998).
[18] J.F. Hergott, M. Kovacev, H. Merdji, C. Hubert, Y. Mairesse, E. Jean, P. Bregger, P. Agostini, B. Carré, and P. Salières, Phys. Rev. A **66**, 021801(R) (2002).
[19] E. Takahashi, Y. Nabekawa, T. Otsuka, M. Obara, and K. Midorikawa, Phys. Rev. A **66**, 021802(R) (2002).
[20] See http://www.cxro.lbl.gov
[21] Ph. Balcou, A.S. Dederichs, M.B. Gaarde, and A. L'Huillier, J. Phys. B **32**, 2973 (1999).
[22] M.B. Gaarde and K.J. Schafer, Phys. Rev. A **65**, 031406 (2002).
[23] M.B. Gaarde and K.J. Schafer, Phys. Rev. Lett. **89**, 213901 (2002).